The Canadian Mineralogist
Vol. 44, pp. 1543-1555 (2006)

THE IMPORTANCE OF COOLING REGIME IN THE FORMATION OF MELT INCLUSIONS IN OLIVINE CRYSTALS IN HAPLOBASALTIC MELTS

SHOSHANA B. GOLDSTEIN[§] AND ROBERT W. LUTH[¶]

C.M. Scarfe Laboratory for Experimental Petrology, Department of Earth and Atmospheric Sciences, University of Alberta, Edmonton, Alberta T6G 2E3, Canada

ABSTRACT

Experiments using synthetic mafic liquids of composition $Fo_{30}Di_{30}An_{40}$ and $Fo_{22}Di_{58}An_{20}$ (wt.%) were conducted to constrain the range of cooling regimes over which melt inclusions form in olivine crystals. In one set of experiments, batches of melt were cooled at rates of 1, 7, 10, 50, 100, and 250°C/h from superliquidus temperatures to 1350 or 1300°C, below the liquidus temperature (1450°C) of both bulk compositions. In a second set of experiments, samples were cooled at rates of 100°C/h and 250°C/h to temperatures of 1300, 1350, or 1400°C, where they were held isothermally for six hours before quenching. Melt inclusions form at cooling rates between 7°C/h and 250°C/h in experiments with no isothermal period. More abundant inclusions formed in the second set of experiments, with an isothermal period. In some cases, melt inclusions form by the simultaneous growth or oriented agglomeration of neighboring platy crystals. This mechanism is consistent with observations of linear trends of inclusions and re-entrants, as well as the composite appearance of platy crystals and long narrow re-entrants between plates.

Keywords: melt inclusions, experiments, igneous petrology, olivine, crystallization, crystal growth, post-entrapment modification, mechanism of trapping.

SOMMAIRE

Nous avons effectué des expériences avec bains fondus silicatés mafiques synthétiques ayant une composition $Fo_{30}Di_{30}An_{40}$ et $Fo_{22}Di_{58}An_{20}$ (proportions pondérales) afin d'établir les taux de refroidissement requis pour former des reliquats magmatiques dans les cristaux d'olivine. Dans une première série d'expériences, les échantillons de liquide ont été refroidis à des taux de 1, 7, 10, 50, 100, et 250°C/h à partir d'une température au dessus du liquidus (>1450°C dans les deux cas) jusqu'à 1350 ou 1300°C. Dans une deuxième série d'expériences, les échantillons ont subi un taux de refroidissement de 100°C/h et 250°C/h jusqu'à 1300, 1350, ou 1400°C, où ils ont été maintenus de façon isothermique pour six heures avant d'être trempés. Les reliquats magmatiques se forment à des taux de refroidissement entre 7°C/h et 250°C/h dans les expériences sans traitement isothermique. Les inclusions vitreuses sont plus abondantes dans la deuxième série d'expériences, avec période isothermique. Dans certains cas, les inclusions vitreuses se forment par croissance simultanée ou bien par agglomération orientée de cristaux en plaquette adjacents. Ce mécanisme concorde avec nos observations de tracés linéaires d'inclusions et de rentrants, ainsi que l'allure composite des cristaux en plaquettes et la présence de longs et étroits rentrants entre les plaquettes.

(Traduit par la Rédaction)

Mots-clés: reliquats magmatiques, expériences, croissance cristalline, pétrologie ignée, olivine, cristallisation, modification post-piégeage, mécanisme de piégeage.

§ *Present address*: Department of Earth and Planetary Sciences, McGill University, Montreal, Quebec H3A 2A7, Canada. *E-mail address*: shoshana@eps.mcgill.ca
¶ *E-mail address*: robert.luth@ualberta.ca

Introduction

Primary melt inclusions are trapped in minerals as the crystals form from a melt (Roedder 1979, 1984). Such inclusions have been used to provide insight into the composition of the melt from which the mineral crystallized (*e.g.,* Anderson 1974, Roedder 1979, Sobolev & Shimizu 1993, Zhaolin 1994, Lu *et al*. 1995, Student & Bodnar 1996, Gioncada *et al*. 1998, Danyushevsky *et al*. 2002a). Analysis of melt inclusions also provides a means of determining the volatile content of the parental magma (*e.g.,* Anderson 1974, Thomas & Klemm 1997, Thomas *et al*. 2000, Roggensack 2001, Massare *et al*. 2002, Cervantes & Wallace 2003, Sirbescu & Nabelek 2003). The utility of melt inclusions is based on the premise that they are samples of the melt in equilibrium with the mineral at the time of entrapment.

Our study is designed to determine the cooling regimes, in particular, constant cooling-rate with and without subsequent isothermal crystallization, in which melt inclusions form in olivine nucleating and growing from an anhydrous model basaltic magma at 1 atmosphere. We address the issue of whether a marked change in growth conditions or the crystallization of incomplete crystals is required to produce melt inclusions. In particular, we wish to discern whether the presence of melt inclusions can itself place any constraints on the cooling rate experienced by a magma.

Background Information

Potential complications in the use of melt inclusions include the entrapment of non-representative melt because of boundary-layer effects adjacent to the growing crystal, and post-entrapment modifications of the melt in the inclusion by crystallization and re-equilibration during cooling. The magnitudes of these issues and their mitigation have been thoroughly considered in the literature (Roedder 1979, 1984, Qin *et al*. 1992, Tait 1992, Lu *et al*. 1995, Nakamura & Shimakita 1998, Danyushevsky *et al*. 2000, 2002a, b, 2004, Gaetani & Watson 2000, 2002, Cottrell *et al*. 2002, Kress & Ghiorso 2004).

Despite the use of melt inclusions as a probe of natural magmatic systems, there are few studies to date that provide insight into the conditions of crystallization required to produce melt inclusions. Roedder (1979, 1984) summarized observational evidence for trapping conditions of melt inclusions, calling on dendritic growth, irregularities in the growth of the crystal face, presence of another mineral on the surface of the growing crystal, or dissolution followed by renewed growth to enable entrapment of melt. Experimental studies of crystal growth and morphology (*cf.* reviews by Kirkpatrick 1975, Lofgren 1980) bear on the issue of trapping of melt inclusions. Kohut & Nielsen (2004) produced plagioclase and olivine crystals containing melt inclusions in a basaltic melt over a range of cooling rates beginning from subliquidus conditions, and Faure & Schiano (2005) studied the formation of melt inclusions in olivine crystals in the CaO–MgO–Al_2O_3–SiO_2 (CMAS) system at one atmosphere.

Olivine is generally the first phase to crystallize from a basalt at low pressures (Osborn & Tait 1952), and would trap liquids early in a liquid line of descent, potentially providing insights into the composition of parental melts. The relationship between cooling rate, degree of undercooling, and crystal morphology has been studied for olivine in both natural and synthetic (CMAS) systems (Donaldson 1976, Faure *et al*. 2003, respectively). Increasing cooling rate and increasing degree of undercooling ($-\Delta T$, the temperature drop below the liquidus prior to quenching) decreases the size of the crystals and changes their morphology from polyhedral or granular to skeletal and ultimately to dendritic and swallowtail crystals. Incomplete outlines of crystals favor the entrapment of melt inclusions if subsequent growth of the crystal encloses the irregularity to produce an inclusion (Anderson 1974, Roedder 1979, Kirkpatrick *et al*. 1981, Faure & Schiano 2005).

Methods

Two compositions of melts, $Fo_{30}Di_{30}An_{40}$ (Composition #1) and $Fo_{22}Di_{58}An_{20}$ (Composition #2) (nominal wt.% in subscripts), with the same liquidus temperature of 1450°C, were selected in the forsterite – diopside – anorthite system (Osborn & Tait 1952), which has a large liquidus field of olivine (Fig. 1). Use of this model system avoided complications of Mg–Fe solid solution in the olivine, and of possible iron or alkali loss from the melt during the experiment. The equilibrium-crystallization sequences of the two compositions differ. Composition #1 crystallizes forsterite until the forsterite–anorthite cotectic is reached at 1290°C, where anorthite begins to crystallize as well. Diopside joins the crystallizing assemblage at 1270°C. In Composition #2, diopside is the second phase to crystallize, at 1340°C on the forsterite–diopside cotectic, with anorthite joining the crystallizing assemblage at the eutectic (1270°C).

The starting materials were prepared using reagent-grade powders of SiO_2, Al_2O_3, MgO, and $CaCO_3$. The $CaCO_3$ powder was dried at 350°C, and the other powders were dried at 1000°C. Appropriate amounts of the four powders were mixed by grinding under ethanol in an agate mortar for 45 minutes, and then dried under a heat lamp. Each mixture was heated in a platinum crucible, with six hours spent at each of 300°C, 500°C, 750°C, and 950°C. Then each mixture was melted at 1550°C for four hours, and quenched in water. The glass slugs were ground to fine powder, remelted for four hours at 1550°C, quenched in water, and reground to fine powder. The analyzed compositions of both starting

materials are slightly more An-rich than their nominal compositions (Table 1), slightly decreasing the liquidus temperatures of both by similar amounts (Fig. 1).

Approximately 20 mg of each starting composition was loaded into separate capsules made of 12 mm lengths of 3-mm-diameter platinum tubing, the bottom end of which had been crimped and welded shut. The capsules were crimped loosely at the top and suspended by a platinum wire. Samples were dried at 110°C overnight before insertion into a $MoSi_2$ tube furnace equipped with a programmable Eurotherm temperature controller and a Pt–Pt13%Rh thermocouple that monitored the temperature of the sample during each run. All experiments were conducted in air. Two series of experiments were conducted. In the CC (Controlled Cooling) series, after a two-hour fusion at superliquidus conditions, the temperature was decreased at a controlled rate to subliquidus conditions, and then the experiment was quenched (CC path in Fig. 2). The CC–ID (Controlled Cooling – Isothermal Dwell) experiments followed the same superliquidus fusion and controlled cooling paths, but were held for six hours isothermally at the subliquidus temperature prior to quenching (CC–ID path in Fig. 2). In all cases, the capsules were quenched in water at the end of the experiment.

After quenching, fragments of each run product were gently crushed under acetone. They were examined in immersion oil (n = 1.650) under transmitted light.

TABLE 1. COMPOSITION AND HOMOGENEITY INDEX OF STARTING GLASSES

	Composition #1, n = 16		Composition #2, n = 24	
	wt.%	H.I.	wt.%	H.I.
SiO_2	48.03 (0.21)	1.63	51.90 (0.13)	1.21
Al_2O_3	15.37 (0.08)	1.00	7.74 (0.07)	1.14
MgO	22.27 (0.13)	1.22	22.77 (0.12)	1.10
CaO	16.00 (0.07)	0.98	19.17 (0.11)	1.30
Total	101.67 (0.18)		101.58 (0.18)	
Fo	29.0		20.9	
Di	29.0		57.2	
An	42.0		21.9	

n: number of points analyzed. One standard deviation of the mean is shown in parentheses. Bulk compositions of the glass are first expressed in wt.% oxides. H.I.: homogeneity index (Boyd *et al.* 1969). The Fo, Di, and An contents were calculated using the MIXING program of IGPET (Carr 2002). In all cases, the sum of squares of the residuals was less than 1.0.

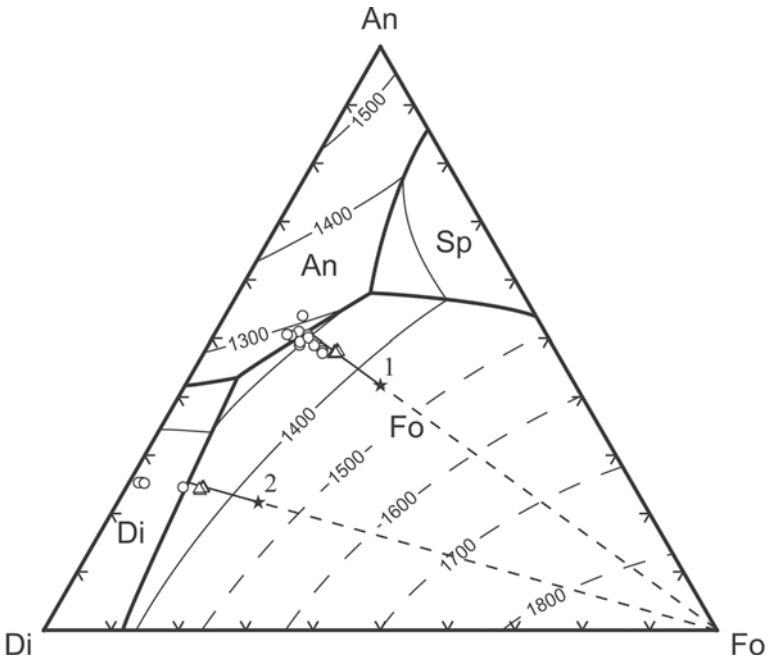

FIG. 1. Liquidus phase diagram of the forsterite – diopside – anorthite pseudoternary system (Osborn & Tait 1952), showing the analyzed compositions of the starting materials (stars). Also shown are the compositions of distal glasses (open triangles) and inclusion glasses (open circles) from run 9. The lines of descent of the liquid for the starting compositions are shown (solid lines). See text for discussion.

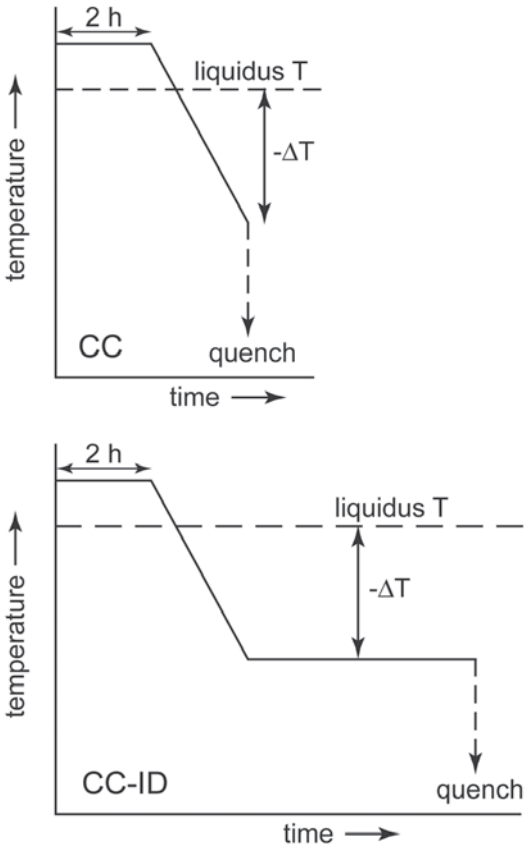

FIG. 2. Schematic temperature – time paths for controlled cooling (CC) and controlled cooling – isothermal dwell (CC–ID) experiments. The solid line represents the experimental path, the horizontal dashed line shows the liquidus temperature of the starting composition, and the vertical dashed line denotes the quenching of the experiment at its completion. Both diagrams also show how we define –ΔT, the temperature from which the experiment is quenched. Adapted from Faure & Schiano (2005).

The presence or absence of true inclusions in crystals (defined by the complete isolation of the inclusion from the exterior of the crystal in three dimensions) and crystal morphology was noted for each composition and run.

Fragments of glass from the synthesis experiment for each starting composition, as well as fragments of the run products from run 9, were mounted in epoxy plugs, ground, and polished for electron-microprobe analysis. Quantitative analyses were conducted with wavelength-dispersive spectroscopy on a JEOL 8900R electron microprobe at an accelerating voltage of 15 kV, a beam current of 15 nA as measured on a Faraday cup, and a beam 3 μm in diameter. We used periclase (MgO), diopside (CaO), kaersutite (Al_2O_3), and Fo_{93} (SiO_2) standards for the analysis of olivine. For the glass analyses, we used the same standards for CaO and Al_2O_3, but Fo_{93} for MgO and a Hawaiian basalt glass for SiO_2. The ZAF correction scheme provided by JEOL was used to process the data. The textural relationships of the inclusions, host crystals, and distal glass in the run products from run 9 were also examined with back-scattered-electron imaging on the electron microprobe.

RESULTS

The run conditions and results for each experiment are given in Table 2. Subsequent measurements of the size of crystals and of the inclusions refer to the longest dimension. No phase other than olivine was encountered in any of the run products.

Melt inclusions

Melt inclusions formed at cooling rates of 7, 10, 50, and 100°C/h in the CC experiments; no inclusions formed at 1°C/h, and inclusions formed at 250°C/h only in Composition 2. Cooling rates of 100 and 250°C/h were chosen for the CC–ID experiments to observe the effect of the isothermal dwell-period on the formation of inclusions. Inclusions were encountered in all CC–ID experiments. In general, crystals from these experiments had significantly more inclusions per crystal (Figs. 3a, b), and there were more crystals with inclusions than in the CC experiments. For example, some crystals from

TABLE 2. EXPERIMENTAL CONDITIONS AND RESULTS

Run #	Cooling Rate (°C/h)	T_q (°C)	–ΔT (°C)	Comp. #1 $Fo_{50}Di_{30}An_{40}$	Comp. #2 $Fo_{22}Di_{58}An_{20}$
			CC experiments (without an isothermal dwell)		
1	7	1350	100	inclusions	inclusions
2	10	1300	150	inclusions	inclusions
3	50	1300	150	inclusions	inclusions
4	100	1300	150	inclusions	inclusions
5	1	1300	150	no inclusions	no inclusions
6	250	1300	150	no inclusions	very few inclusions
			CC-ID experiments (with a 6 h isothermal dwell)		
7	250	1300	150	inclusions	inclusions
8	100	1300	150	inclusions	inclusions
9	250	1350	100	inclusions	inclusions
10	100	1350	100	inclusions	inclusions
11	250	1400	50	inclusions; few crystals	inclusions; few crystals
12	100	1400	50	inclusions; very few crystals	inclusions; very few crystals

Initial dwell-temperature was 1500°C for run 1, 1475°C for others. Initial dwell-time was 2 h for all runs. T_q: Temperature from which the experiment was quenched. –ΔT represents the undercooling ($T_q - T_{liquidus}$).

the CC–ID experiments contain up to 15 inclusions, whereas crystals from the CC experiments contain up to three, but typically one inclusion per crystal.

Inclusions are typically circular or oval (Fig. 3a), or less commonly tubular (Figs. 3b, c). Rarely, inclusions with an irregular morphology were observed (Fig. 3d). Patterns of inclusions were observed in some crystals with multiple inclusions. In some crystals, inclusions align along a common direction and form a linear trend, either parallel or perpendicular to the long axes of the inclusions (Figs. 4a, b). In other crystals, oval or elongate tubular inclusions are aligned parallel to an elongate, tubular embayment that we shall refer to as a re-entrant. We use "re-entrant" rather than "embayment" to avoid any implication of formation by reaction with or dissolution in the melt. These inclusions may be either in line with (Fig. 4c) or adjacent to (Fig. 4d) the re-entrant. In one crystal, two re-entrants from opposite faces align along the length of a crystal (Fig. 4e). In another crystal, several inclusions occur along a linear discontinuity in the crystal structure (Fig. 4f), which might represent a previous fracture or crystal boundary.

Crystal size and morphology

In general, crystals were larger in the CC–ID experiments than in the CC ones, consistent with continued growth during the isothermal dwell period. We observed polyhedral, granular, hopper, and plate crystals in our experiments. Hopper crystals were not commonly encountered, but were present even at cooling rates as low as 10°C/h. Polyhedral crystals were most abundant in run 5 (1°C/h), but both polyhedral and granular crystals formed commonly, at a variety of cooling rates (Figs. 3, 4).

In some cases, platy crystals have grown together (Figs. 5a, b), as described by Donaldson (1976). In other cases, the parallelism of re-entrants (Fig. 4e) or the alignment of re-entrants with tubular inclusions (Fig. 4c) may be the result of coalescence of platy crystals. In one case (Fig. 5c), we saw two crystals that appear to have coalesced edgewise.

Electron-microprobe results

We evaluated the homogeneity of the starting glasses using the test of Boyd *et al*. (1969). Their homogeneity index is defined as the ratio of the standard deviation of the count data for a given component to the standard deviation expected from Poisson counting statistics ($\sqrt{N}$, where N represents the number of counts). They considered that a component is homogeneous if the homogeneity index is ≤ 3. The homogeneity indices are in the range 0.98–1.63 for SiO_2, Al_2O_3, MgO, and CaO for both starting compositions (Table 1), and thus both glasses are homogeneous by their criterion.

Olivine crystals analyzed from run 9 are stoichiometric and contain some Ca (Table 3). The measured Ca contents, and the lower contents in olivine crystals from Composition 1 relative to those in Composition 2, agree with values calculated from the model of Libourel (1999) for Ca partitioning between olivine and melt for our melt compositions at 1350°C. This agreement is consistent with equilibrium partitioning of Ca between melt and olivine during crystal growth.

The glasses distal (>70 μm away) with respect to the olivine crystals in both compositions in run 9 are enriched in Si, Al, and Ca and depleted in Mg relative to the starting compositions (Table 3), and have compositions consistent with those expected for crystallization at 1350°C, as deduced from the phase diagram (Fig. 1). The compositions of melt inclusions from both Compositions 1 and 2 in run 9 are more variable than those of their respective distal glasses (Table 4). The inclusion glasses are depleted in Mg and enriched in Al and Ca relative to the distal glasses (Fig. 1).

DISCUSSION

Analysis of results

Inclusions form in olivine in CC experiments at cooling rates ranging from 7°C/h to 250°C/h, but do not form at a rate of 1°C/h. In the CC experiment at a cooling rate of 250°C/h, the majority of crystals have elongate, tubular re-entrants, but only two inclusions were observed in Composition 2, and none were observed in Composition 1. This observation shows that it is possible for inclusions to form at this cooling rate, but the probability is quite low. Thus 250°C/h is likely close to the maximum rate of cooling that will allow the trapping of melt as inclusions in crystals of these morphologies. This difference in behavior between the two compositions may be a result of their differing compositions of melt.

Observations of crystal morphology in our experiments are consistent with previous observations that higher rates of cooling result in more incomplete shapes of crystals because growth rate increases faster than the diffusion rate (Donaldson 1976, Faure *et al*. 2003). The most incomplete crystal form observed in runs 1 to 6 is plate olivine (Donaldson 1976), which formed at cooling rates of ≥50°C/h (Figs. 5a, b). These plates, which resemble decks of cards, may result from growth of parallel plates from a single nucleus (P. Roeder, pers. commun., 2005), or from coalescence of neighboring crystals. More incomplete skeletal and dendritic forms would be expected only at higher rates of cooling (Faure *et al*. 2003).

In the CC–ID experiments (runs 7 to 10), both crystals and inclusions were abundant, and crystals with polyhedral, granular, and plate morphologies were observed in both compositions. There were slightly

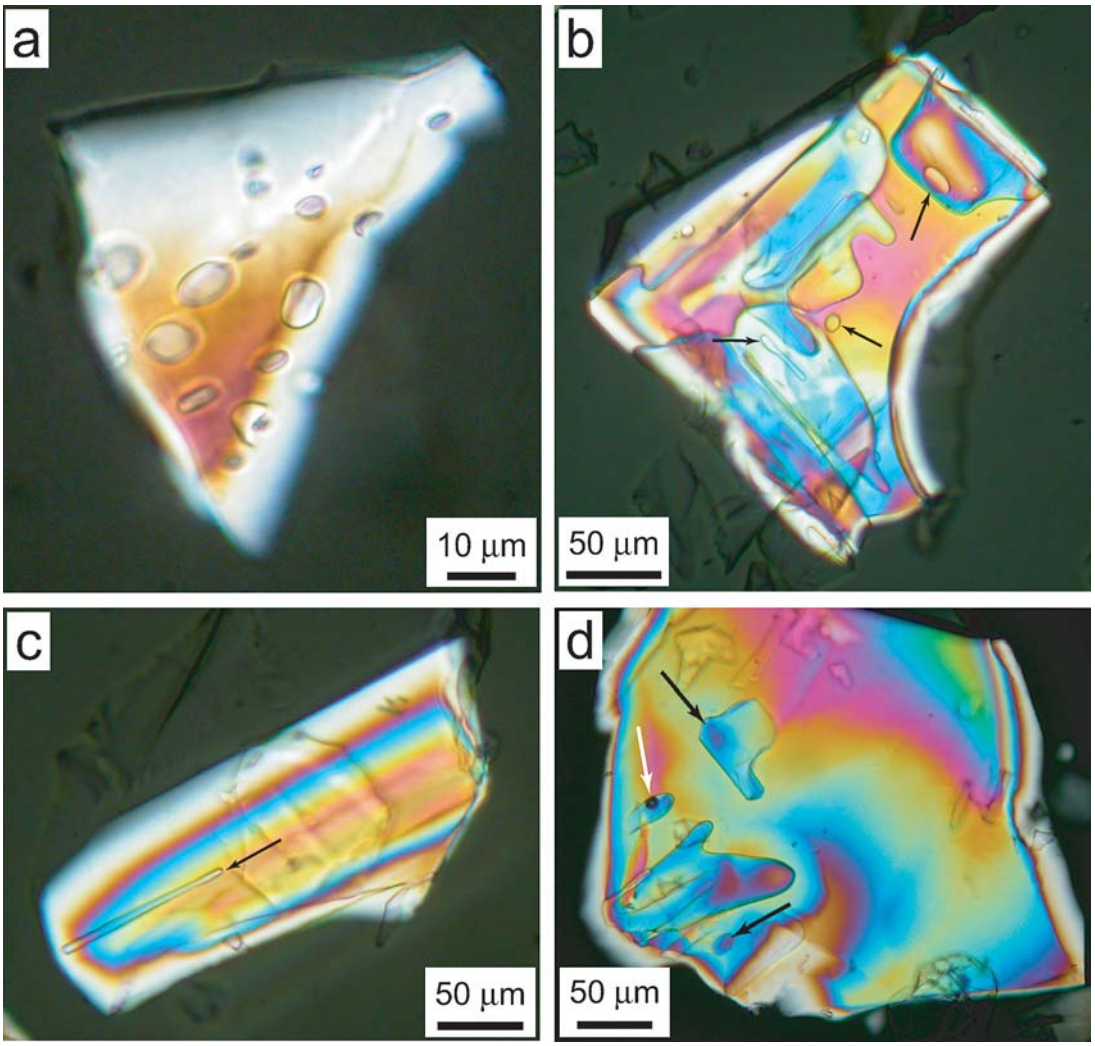

FIG. 3. a) Crystal from a CC–ID experiment (run 7, Composition 2) hosting ~15 inclusions. Crystal is 77 μm across, typical inclusion is ~9 μm. b) Crystal from a CC–ID experiment (run 9, Composition 1) hosting oval and tubular melt inclusions (arrows). Crystal is 216 μm, near-circular inclusion in the center of the crystal is ~8 μm. c) Crystal hosting a tubular inclusion from run 8, Composition 2. Crystal is 208 μm across, inclusion is 77 μm. d) Crystal from run 1, Composition 2 containing an irregularly shaped inclusion (72 μm) and oval inclusions, one containing a shrinkage bubble (white arrow). Circular inclusion marked by arrow is 16 μm. All photomicrographs are in crossed polars, and have been cropped to focus on the crystal of interest. Arrows show locations of inclusions.

fewer crystals in runs 9 and 10 ($-\Delta T = 100°C$) relative to runs 7 and 8 ($-\Delta T = 150°C$). The run products from runs 11 and 12 ($-\Delta T = 50°C$) are similar to each other, but quite different from runs 7 to 10 in that very few crystals formed. Crystals that formed in runs 11 and 12 are generally small (30–40 μm) and granular. Despite the small number of crystals in the run products of runs 11 and 12, inclusions in the crystals are relatively common. Each slide examined from these two experiments also contains one or two large crystals, ~250 to ~400 μm. This bimodal distribution of crystal size observed in runs 11 and 12 may result from coarsening processes such as Ostwald ripening (Park & Hanson 1999). No such bimodal distribution was observed in runs 7 to 10, which had identical isothermal periods but larger undercoolings. This difference may reflect a dependence of the coarsening on the degree of undercooling.

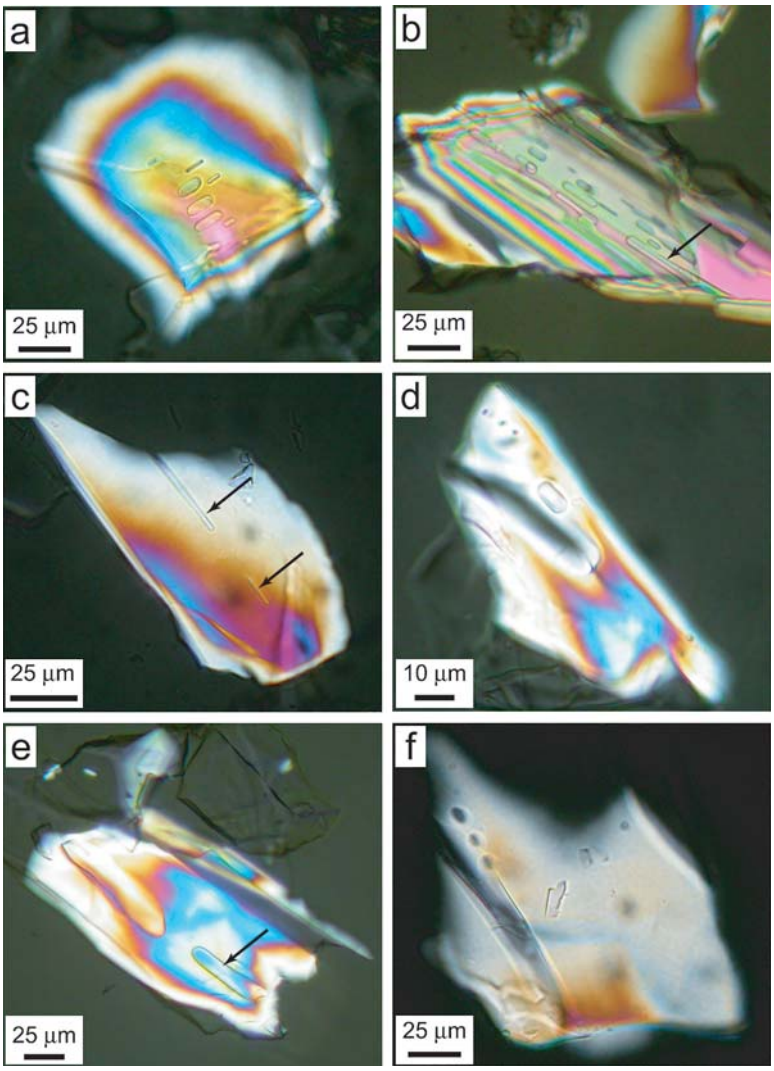

FIG. 4. a) Coplanar inclusions oriented preferentially in a linear trend perpendicular to the long axes of the inclusions. Crystal is from run 9, Composition 1 and is 122 μm, inclusions range from 5 to 11 μm. b) Coplanar tubular inclusions aligned parallel to the long axes of the inclusions. More inclusions with the same orientation exist in other planes of focus. The inclusion at lower right (arrow) may be a re-entrant; it is not clear that it is isolated from the surrounding melt. Crystal is from run 10, Composition 2 and is 200 μm, but only 145 μm is shown. c) An elongate, tubular inclusion is aligned with a tubular re-entrant in a crystal from run 3, Composition 1. Crystal is 125 μm across, inclusion is 13 μm. d) Several inclusions aligned with each other parallel to an adjacent re-entrant in a crystal from run 7, Composition 2. Crystal is 96 μm across, largest inclusion is ~10 μm across, re-entrant is ~30 μm long. e) Two re-entrants from opposite faces align along the length of a crystal from run 8, Composition 2. Crystal is 184 μm across, larger re-entrant is 80 μm, smaller re-entrant is 56 μm, inclusion is 13 μm. f) Three inclusions align along a linear discontinuity in the crystal from run 2, Composition 1. Crystal is 163 μm, largest inclusion is 9.6 μm.

Despite the difference in the abundance of crystals, the ratio of inclusions to crystals is comparable in all six CC–ID experiments, and so the temperature of the isothermal dwell does not appear to exert significant control on the formation of inclusions. The abundance of inclusions formed in the CC–ID experiments, however, is noticeably greater than in the CC experiments, as outlined above. Although inclusions are less abundant in the CC experiments, re-entrants are more common than in the CC–ID experiments. We infer that the isothermal period in the CC–ID experiments allowed crystal growth to close some re-entrants and trap melt completely within the crystal. Annealing of a single re-entrant may form multiple, aligned inclusions (*e.g.,* Fig. 4b).

It is noteworthy that crystals containing melt inclusions, including some with multiple inclusions, formed in the CC–ID experiments with a 250°C/h cooling rate, a rate that was not conducive to the formation of inclusion-bearing crystals in the CC experiments. This difference requires that melt inclusions form during the isothermal portion of the CC–ID experiments by continued growth or coalescence of grains.

The glasses distal to the olivine crystals in the products from run 9 have compositions consistent with crystallization of olivine at the dwell temperature of the experiment (Fig. 1). The compositions of the melt inclusions are more evolved along the two lines of descent of the liquid than are the distal glasses (Fig. 1). Indeed, the compositions of several melt inclusions lie on, or even across, the forsterite–anorthite or forsterite–diopside cotectics (Fig. 1), which cannot be achieved by equilibrium crystallization at 1350°C. Such olivine-depleted melt compositions might be the result of trapping of boundary-layer melt depleted in Fo because crystal growth outstripped rates of diffusion. Such a melt, however, would not be in chemical equilibrium with the growing crystal and should dissolve olivine until equilibrium was re-established. We interpret the compositions of the melt inclusions instead to result from metastable post-entrapment crystallization of olivine from the melt. The absence of daughter crystals in the melt inclusions is consistent with crystallization of olivine onto the walls of the inclusion (*cf.* discussion in Roedder 1979). Between ~2 and ~12 wt.% olivine must be added to the composition of a given inclusion for its composition to match that of the distal glass (Table 5). However, we found no correlation between inclusion size, as measured in the plane of the section through the inclusion, and the amount of crystallization. This result contrasts with the observations of Danyushevsky *et al.* (2003) on melt inclusions in olivine crystals from MORB. This difference may arise because nearly all of our inclusions are smaller than 200 μm, the minimum size they found that was required to mitigate the effect of this crystallization.

The timing of this post-entrapment crystallization is unconstrained, but there is no driving force for crystallization that would change the composition of the melt relative to the composition of the distal glass during the isothermal dwell. Therefore, it seems most likely that this crystallization occurred as the experiment was quenched. Metastable growth of olivine during rapid cooling has been observed in previous crystal-growth studies (Kirkpatrick *et al.* 1981, 1983). If this is the case, such quench crystallization may also occur in heating experiments designed to re-homogenize melt inclusions, raising the possibility that such "re-homogenized" melt inclusions of the size we produced may still not be representative of the original trapped melt, unlike larger ones (*e.g.,* Danyushevsky *et al.* 2003).

Comparison of results with previous studies

Kohut & Nielsen (2004) used a natural N-MORB glass as their starting composition, seeded with $Fo_{91–92}$

TABLE 3. AVERAGE COMPOSITIONS OF OLIVINE CRYSTALS AND DISTAL GLASS

	Composition #1		Composition #2	
n	Olivine 23	Distal glass 9	Olivine 19	Distal glass 6
SiO_2	41.31 (0.22)	48.07 (0.24)	41.35 (0.22)	52.32 (0.15)
Al_2O_3	0.19 (0.09)	17.23 (0.08)	0.06 (0.02)	8.60 (0.05)
MgO	57.07 (0.20)	17.23 (0.05)	56.72 (0.22)	18.43 (0.12)
CaO	0.52 (0.02)	17.90 (0.13)	0.78 (0.04)	21.40 (0.21)
Total	99.11 (0.26)	100.44 (0.26)	98.912 (0.27)	100.76 (0.44)
Fo		19.6		11.3
Di		32.8		64.4
An		47.6		24.3

Olivine crystals analyzed from run 9. *n*: number of points analyzed. One standard deviation of the mean is shown in parentheses. Bulk compositions are first expressed in wt.% oxides, then those of the glass are recast into Fo, Di and An contents (wt.%) as explained in Table 1.

TABLE 4. REPRESENTATIVE COMPOSITIONS OF MELT IN INCLUSIONS

	Composition #1					Composition #2				
point	3-7	3-4	3-10	3-1	4-6	1-4	3-2	2-3	3-1	2-4
SiO_2	48.17	48.23	48.65	46.24	48.61	52.22	52.99	52.58	52.40	52.50
Al_2O_3	17.24	17.69	18.29	18.76	18.35	8.54	9.10	9.13	9.08	9.31
MgO	16.67	15.65	14.63	13.89	13.39	17.17	14.95	14.74	14.41	13.36
CaO	18.46	18.84	19.19	19.76	20.02	21.86	23.86	23.87	23.84	24.62
Total	100.54	100.41	100.77	98.65	100.38	99.79	100.89	100.33	99.72	99.80
Fo	17.8	15.9	14.1	12.5	11.0	8.6	2.5	2.1	1.6	0.0
Di	34.8	35.4	35.4	36.5	38.5	67.0	72.4	72.7	73.2	73.5
An	47.4	48.7	50.4	51.0	50.5	24.4	25.1	25.2	25.2	26.5

Bulk compositions are first expressed in wt.% oxides, then are recast into Fo, Di and An contents (wt.%) as explained in Table 1.

olivine to ensure saturation in olivine. Their experiments were conducted in plagioclase crucibles at 1 atm, with oxygen fugacity fixed at the QFM buffer, with an initial subliquidus equilibration at 1300°C. Samples were then cooled at rates of 60, 300, and 600°C/h to 1230° and 1210°C in CC and CC–ID-type experiments (Fig. 2). In the CC–ID experiments, the isothermal dwell periods were 0, 1, 3, 6, and 24 h at 1230°C, and 6 h at 1210°C. An additional run was cooled at 60°C/h to 1230°C and held there for 116 h (Kohut & Nielsen 2004). Plagioclase crystals were observed in every run, but olivine was not seen in any of their experiments that had isothermal dwell-times of less than 6 h, except for one with a 3 h dwell. This observation suggests that the olivine seeds must have dissolved completely during the initial equilibration step at 1300°C. In their experiments with isothermal dwells ≥ 6 h, olivine crystals, some with melt inclusions, were found, consistent with nucleation and growth of olivine during the isothermal period. The absence of olivine crystals in experiments with short isothermal periods contrasts with our observations of olivine nucleation and growth in CC experiments as well as CC–ID ones. This difference may be the result of undersaturation of olivine or the lower degrees of undercooling in their experiments, which would inhibit nucleation (Donaldson 1979). Alternatively, the difference in behavior may be the result of differing viscosities of the melts, given that higher viscosity inhibits nucleation (Donaldson 1979). At 1300°C, the calculated viscosity of their melt is 14.4 Pa•s (model of Giordano & Dingwell 2003, 2004), well above the calculated viscosities of our melts at their liquidus temperatures, 0.58 Pa•s (Composition 1) and 0.45 Pa•s (Composition 2).

Kohut & Nielsen (2004) found inclusions in every run that nucleated olivine crystals, including those at higher cooling-rates than those used in our study. They did not, however, do any experiments at the low cooling rate (1°C/h) at which we observed olivine growth without inclusion formation. In their study, and like us, they did not find as systematic a dependence of crystal morphology on cooling rate and undercooling as did Donaldson (1976) and Faure *et al*. (2003). Kohut & Nielsen (2004) observed polyhedral, granular, hopper, and intergrown crystals, commonly with two morphologies in a given experiment.

Faure & Schiano (2005) examined olivine growth and formation of melt inclusions in a liquid in the system CMAS. The composition they studied is more silica-rich (normative composition An 39.1, Di 36.8, Fo 17.1, Qtz 7.0 wt.%) and has a lower liquidus temperature (1342°C) than either of ours. They conducted CC experiments at 1, 225, 525, 991, and 1890°C/h to undercoolings of 44–176°C. They also used a modified CC procedure, with two cooling rates. The initial slow-cooling step (2°C/h) led to polyhedral crystals that were then overgrown by skeletal or dendritic features at a more rapid cooling-rate (1639–1730°C/h). These experiments were then quenched from temperatures of 1082–1167°C. They did not carry out any CC–ID-type experiments.

Their CC experiment at 1°C/h produced polyhedral crystals with embayments and melt inclusions (their Fig. 3). The inclusions are typically irregular in shape and randomly distributed in the host crystal. They proposed that the polyhedral crystals grew by interface-controlled growth, and that a "spiral growth interaction process" (Faure & Schiano 2005, p. 894) forms embayments that are then enclosed by continued growth. These experiments are comparable to our slower CC experiments, and it is notable that we found no melt inclusions in our CC experiment cooled at 1°C/h. This difference suggests that there may be a compositional control on the minimum rate of cooling that produces melt inclusions.

Faure & Schiano (2005) found that the composition of the glass in the inclusions in the polyhedral crystals is identical to that analyzed at a distance of >100 μm from the crystal. They did not report any post-entrapment modification such as we observed. This difference may simply result from a difference in quench rates (with theirs more rapid) or from the difference in composition. The combination of a more silicic composition and lower temperatures means that the viscosity of their melt is greater than ours [at its liquidus temperature, it is calculated to be 4.26 Pa•s with the model of Giordano & Dingwell (2003, 2004) ~10× higher than either of ours at their liquidus temperature].

Interestingly, Faure & Schiano (2005) found that the compositions of melt inclusions formed in dendritic and skeletal crystals and overgrowths in their more rapidly cooled experiments differ markedly from the compositions of the distal glasses. This contrast with the results from the melt inclusions in the polyhedral crystals led them to propose that boundary-layer effects are important in such cases, and that it is the mode of

TABLE 5. POST-ENTRAPMENT CRYSTALLIZATION OF OLIVINE AND INCLUSION SIZE

Analysis point	Inclusion size (μm)	Olivine (wt.%)	Analysis point	Inclusion size (μm)	Olivine (wt.%)
Composition #1			Composition #2		
1-1	26	6.0	1-4	52	2.7
2-1	20	7.2	2-3	18	8.9
3-1	23	7.9	2-4	20	11.7
3-2	75	6.3	3-1	11	9.4
3-4	71	3.9	3-2	13	8.6
3-5	71	2.5			
3-6	221	2.0			
3-7	221	1.6			
3-10	160	6.2			
3-11	160	5.8			
4-2	70	9.3			
4-3	70	8.3			
4-6	48	8.9			

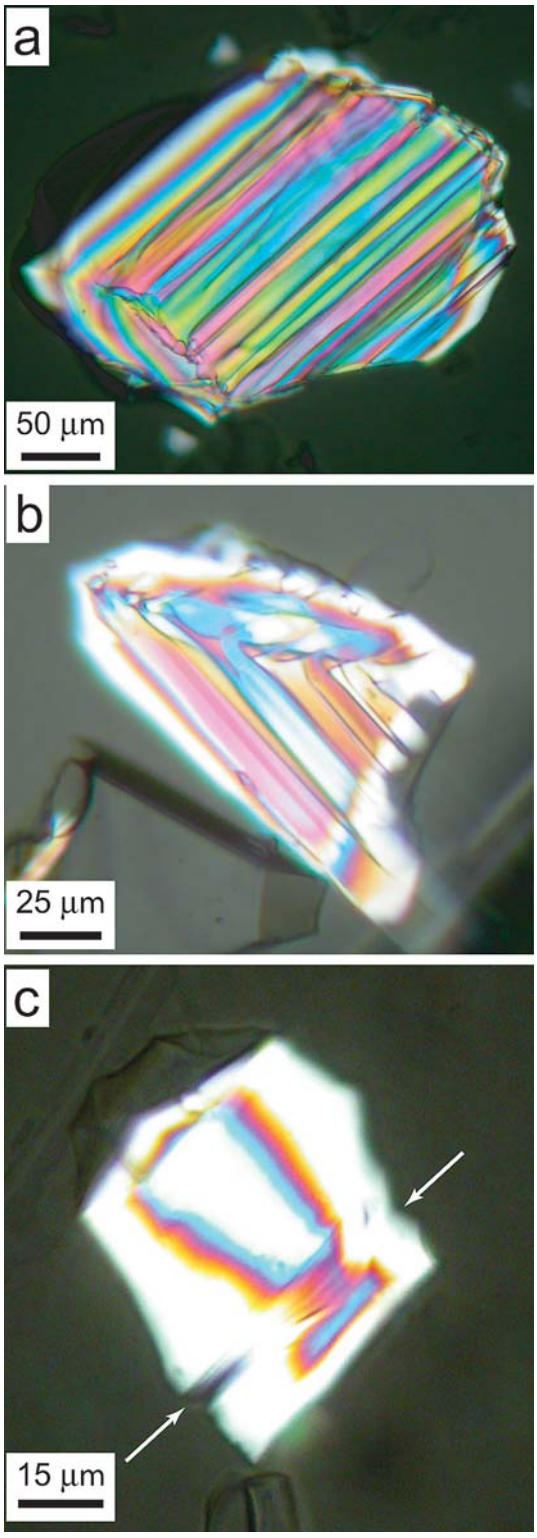

crystal growth during inclusion entrapment, not size of inclusion, that dictates whether the inclusion is a representative sample of the parent melt.

Significance

In our experiments, melt inclusions form in olivine crystals cooled at rates between ~7°C/h and ~250°C/h. Under these conditions, polyhedral and granular morphologies dominate, rather than skeletal or dendritic forms. These cooling rates may be higher than those that occur in many natural situations (Cooper *et al.* 2001, Kohut & Nielsen 2004). There are situations characterized by faster cooling-rates, such as extrusion of pillow basalts (*e.g.,* Faure & Schiano 2004 and references therein), but even dike transport can be associated with cooling rates comparable to those in our study. For example, Thornber (2001) studied growth of olivine crystals in basaltic magma moving from a magma chamber beneath the summit of Kīlauea volcano through the dike conduit along the East Rift Zone. He estimated that the magma cooled at 2°C/h during this transit. A critical point is that melt inclusions formed in our experiments in crystals that did not have skeletal or dendritic morphologies, demonstrating that such incomplete forms are not required to form melt inclusions. In addition, the observation that crystals with multiple inclusions form during periods of isothermal crystal-growth, rather than during periods of cooling, may be used to place constraints on natural temperature–time profiles. In various tectonic settings, basaltic magma traverses the lithosphere *via* fractures or conduits and collects in the crust in magma chambers or melt lenses prior to eruption (Kohut & Nielsen 2004, and references therein). Stagnation of the magma in these settings is one method of achieving essentially isothermal crystallization in nature, proxying the "ID" stage of our CC–ID experiments.

Formation of melt inclusions by agglomeration

Several lines of evidence from this study support the possibility that melt inclusions form when pre-existing crystals grow together. The greater abundance both of

FIG. 5. a) Stacked platy crystals from run 3, Composition 1. Crystal is 264 µm across. The variable birefringence is presumably a result of glass between the individual plates. b) Stacked platy crystals from run 6, Composition 2. Individual plates have grown together. Crystal is 140 µm across. c) Two crystals that have grown once they made contact, forming a re-entrant (lower left) similar to those that were sealed with continued growth. White arrows delineate the interface between the two crystals. Crystal is 54 µm measured perpendicular to the re-entrant.

crystals with melt-inclusions and crystals containing multiple melt-inclusions in the CC–ID experiments relative to the CC ones is evidence that processes of continued growth or coalescence during the isothermal period are conducive to the formation of melt inclusions. The trapping of melt as inclusions by agglomeration of crystals has been observed in annealing experiments in partially molten carbonate systems (Renner *et al*. 2002). We suggest that melt becomes trapped in olivine crystals when preformed crystals become aligned parallel to each other and grow together to form a larger crystal. This process produces re-entrants initially, which are then enclosed by continued crystallization (annealed) to form melt inclusions. Although we observed many re-entrants in the CC experiments (runs 1–6) and found inclusions to be rarer, inclusions are much more prevalent in the CC–ID experiments, and re-entrants less so. The isothermal interval of runs 7 to 12 likely acted to anneal many re-entrants to produce encapsulated inclusions of melt and allowed agglomeration or coalescence of crystals, possibly by synneusis (Schwindinger & Anderson 1989, Schwindinger 1999). The alignment of such crystals is similar to what occurs in the formation of twins during crystal growth (Cahn 1954, Nespolo & Ferraris 2004), which arise by the oriented attachment or agglutination of pre-formed crystals. Alternatively, as noted previously, the plates of olivine may have a common nucleus and have grown in the same relative orientation from the start.

Experiments in which olivine growth and inclusion entrapment are observed *in situ* (Sunagawa 1992) would be needed to resolve the issue of platy olivine growth as related to inclusion entrapment.

Conclusions

1) Melt inclusions form at cooling rates between ~7°C/h and ~250°C/h in CC experiments.

2) Melt inclusions form at cooling rates of 100°C/h and 250°C/h in CC–ID experiments that had a 6-hour isothermal dwell at various undercoolings.

3) Observed morphologies of crystals include polyhedral, granular, hopper, and plate olivine, with higher rates of cooling generally producing more incomplete morphologies.

4) Comparisons of the composition of the included melt with that of the glass distal to the crystals demonstrate that there was significant post-entrapment modification of included melt by crystallization of forsterite on the wall of the inclusion during quenching of the experiment.

5) Crystals formed during the CC–ID experiments tend to be larger and contain more inclusions than those from CC experiments. The greater number of inclusions in the former is attributed to annealing of re-entrants by continued growth during the isothermal dwell period, and to coalescence of parallel plates of olivine that trap melt as the plates grow together.

Acknowledgements

This paper is based on the first author's B.Sc. Honours Thesis. This research is supported by NSERC through a USRA to S.G. and a Discovery Grant to R.W.L. Assistance with the electron microprobe by Sergei Matveev is greatly appreciated. We thank L.V. Danyushevsky and P.L. Roeder for their constructive reviews, which improved this contribution very much. Editorial comments by R.F. Martin significantly improved the presentation and content of this paper.

References

Anderson, A.T. (1974): Evidence for a picritic, volatile-rich magma beneath Mt. Shasta, California. *J. Petrol*. **15**, 243-267.

Boyd, F.R., Finger, L.W. & Chayes, F. (1969): Computer reduction of electron-probe data. *Carnegie Inst. Wash., Yearb*. **67**, 210-215.

Cahn, R.W. (1954): Twinned crystals. *Adv. Physics* **3**, 363-445.

Carr, M.J. (2002): *IGPET for Windows*.: Terra Softa Inc., 155 Emerson Road, Somerset, New Jersey 08873, U.S.A.

Cervantes, P. & Wallace, P.J. (2003): The role of H_2O in subduction-zone magmatism: new insights from melt inclusions in high-Mg basalts from central Mexico. *Geology* **31**, 235-238.

Cooper, K.M., Reid, M.R., Murrell, M.T. & Clague, D.A. (2001): Crystal and magma residence at Kilauea Volcano, Hawaii: $^{230}Th - ^{226}Ra$ dating of the 1955 east rift eruption. *Earth Planet. Sci. Lett*. **184**, 703-718.

Cottrell, E., Spiegelman, M. & Langmuir, C.H. (2002): Consequences of diffusive reequilibration for the interpretation of melt inclusions. *Geochemistry Geophysics Geosystems* **3**(5), DOI: 10.1029/2001GC000205.

Danyushevsky, L.V., Della-Pasqua, F.N. & Sokolov, S. (2000): Re-equilibration of melt inclusions trapped by magnesian olivine phenocrysts from subduction-related magmas: petrological implications. *Contrib. Mineral. Petrol*. **138**, 68-83.

Danyushevsky, L.V., Leslie, R.A.J., Crawford, A.J. & Durance, P. (2004): Melt inclusions in primitive olivine phenocrysts: the role of localized reaction processes in the origin of anomalous compositions. *J. Petrol*. **45**, 2531-2553.

Danyushevsky, L.V., McNeill, A.W. & Sobolev, A.V. (2002a): Experimental and petrological studies of melt inclusions in phenocrysts from mantle-derived magmas: an overview of techniques, advantages and complications. *Chem. Geol*. **183**, 5-24.

DANYUSHEVSKY, L.V., PERFIT, M.R., EGGINS, S.M. & FALLOON, T.J. (2003): Crustal origin for coupled 'ultra-depleted' and 'plagioclase' signatures in MORB olivine-hosted melt inclusions: evidence from the Siqueiros Transform Fault, East Pacific Rise. *Contrib. Mineral. Petrol.* **144**, 619-637.

DANYUSHEVSKY, L.V., SOKOLOV, S. & FALLOON, T.J. (2002b): Melt inclusions in olivine phenocrysts: using diffusive re-equilibration to determine the cooling history of a crystal, with implications for the origin of olivine-phyric volcanic rocks. *J. Petrol.* **43**, 1651-1671.

DONALDSON, C.H. (1976): An experimental investigation of olivine morphology. *Contrib. Mineral. Petrol.* **57**, 187-213.

DONALDSON, C.H. (1979): An experimental investigation of the delay in nucleation of olivine in mafic magmas. *Contrib. Mineral. Petrol.* **69**, 21-32.

FAURE, F. & SCHIANO, P. (2004): Crystal morphologies in pillow basalts: implications for mid-ocean ridge processes. *Earth Planet. Sci. Lett.* **220**, 331-344.

FAURE, F. & SCHIANO, P. (2005): Experimental investigation of equilibration conditions during forsterite growth and melt inclusion formation. *Earth Planet. Sci. Lett.* **236**, 882-898.

FAURE, F., TROLLIARD, G., NICOLLET, C. & MONTEL, J.-M. (2003): A developmental model of olivine morphology as a function of the cooling rate and the degree of undercooling. *Contrib. Mineral. Petrol.* **145**, 251-263.

GAETANI, G.A. & WATSON, E.B. (2000): Open system behavior of olivine-hosted melt inclusions. *Earth Planet. Sci. Lett.* **183**, 27-41.

GAETANI, G.A. & WATSON, E.B. (2002): Modeling the major-element evolution of olivine-hosted melt inclusions. *Chem. Geol.* **183**, 25-41.

GIONCADA, A., CLOCCHIATTI, R., SBRANA, A., BOTTAZZI, P., MASSARE, D. & OTTOLINI, L. (1998): A study of melt inclusions at Vulcano (Aeolian Islands, Italy): insights on the primitive magmas and on the volcanic feeding system. *Bull. Volcanol.* **60**, 286-306.

GIORDANO, D. & DINGWELL, D.B. (2003): Non-Arrhenian multicomponent melt viscosity: a model. *Earth Planet. Sci. Lett.* **208**, 337-349.

GIORDANO, D. & DINGWELL, D.B. (2004): Erratum to "Non Arrhenian multicomponent melt viscosity: a model". *Earth Planet. Sci. Lett.* **221**, 449.

KIRKPATRICK, R.J. (1975): Crystal growth from melt: a review. *Am. Mineral.* **60**, 798-814.

KIRKPATRICK, R.J., KUO, LUNG-CHUAN & MELCHIOR, J. (1981): Crystal growth in incongruently-melting compositions – programmed cooling experiments with diopside. *Am. Mineral.* **66**, 223-241.

KIRKPATRICK, R.J., RECK, B.H., PELLY, I.Z. & KUO, LUNG-CHUAN (1983): Programmed cooling experiments in the system MgO–SiO_2: kinetics of a peritectic reaction. *Am. Mineral.* **68**, 1095-1101.

KOHUT, E. & NIELSEN, R.L. (2004): Melt inclusion formation mechanisms and compositional effects in high-An feldspar and high-Fo olivine in anhydrous mafic silicate liquids. *Contrib. Mineral. Petrol.* **147**, 684-704.

KRESS, V.C. & GHIORSO, M.S. (2004): Thermodynamic modeling of post-entrapment crystallization in igneous phases. *J. Volcanol. Geotherm. Res.* **137**, 247-260.

LIBOUREL, G. (1999): Systematics of calcium partitioning between olivine and silicate melt: implications for melt structure and calcium content of magmatic olivines. *Contrib. Mineral. Petrol.* **136**, 63-80.

LOFGREN, G.E. (1980). Experimental studies on the dynamic crystallization of silicate melts. *In* Physics of Magmatic Processes (R.B. Hargraves, ed.). Princeton University Press, Princeton, New Jersey (487-551).

LU, F.Q., ANDERSON, A.T. & DAVIS, A.M. (1995): Diffusional gradients at the crystal/melt interface and their effect on the composition of melt inclusions. *J. Geol.* **103**, 591-597.

MASSARE, D., MÉTRICH, N. & CLOCCHIATTI, R. (2002): High-temperature experiments on silicate melt inclusions in olivine at 1 atm: inference on temperatures of homogenization and H_2O concentrations. *Chem. Geol.* **183**, 87-98.

NAKAMURA, M. & SHIMAKITA, S. (1998): Dissolution origin and syn-entrapment compositional change of melt inclusion in plagioclase. *Earth Planet. Sci. Lett.* **161**, 119-133.

NESPOLO, M. & FERRARIS, G. (2004): The oriented attachment mechanism in the formation of twins – a survey. *Eur. J. Mineral.* **16**, 401-406.

OSBORN, E.F. & TAIT, D.B. (1952): The system diopside – forsterite – anorthite. *Am. J. Sci.* **250**, 413-433.

PARK, Y. & HANSON, B. (1999): Experimental investigation of Ostwald-ripening rates of forsterite in the haplobasaltic system. *J. Volcanol. Geotherm. Res.* **90**, 103-113.

QIN, ZHEN-WEI, LU, FANG-QIONG & ANDERSON, A.T., JR. (1992): Diffusive reequilibration of melt and fluid inclusions. *Am. Mineral.* **77**, 565-576.

RENNER, J., EVANS, B. & HIRTH, G. (2002): Grain growth and inclusion formation in partially molten carbonate rocks. *Contrib. Mineral. Petrol.* **142**, 501-514.

ROEDDER, E. (1979): Origin and significance of magmatic inclusions. *Bull. Minéral.* **102**, 487-510.

ROEDDER, E. (1984): Fluid Inclusions. *Rev. Mineral.* **12**.

ROGGENSACK, K. (2001): Unraveling the 1974 eruption of Fuego volcano (Guatemala) with small crystals and their young melt inclusions. *Geology* **29**, 911-914.

SCHWINDINGER, K.R. & ANDERSON, A.T. (1989): Synneusis of Kilauea Iki olivines. *Contrib. Mineral. Petrol.* **103**, 187-198.

SCHWINDINGER, K.R. (1999): Particle dynamics and aggregation of crystals in a magma chamber with application to Kilauea Iki olivines. *J. Volcanol. Geotherm. Res.* **88**, 209-238.

SIRBESCU, M.-L.C. & NABELEK, P.I. (2003): Crustal melts below 400°C. *Geology* **31**, 685-688.

SOBOLEV, A.V. & SHIMIZU, N. (1993): Ultra-depleted primary melt included in an olivine from the Mid-Atlantic Ridge. *Nature* **363**, 151-154.

STUDENT, J.J. & BODNAR, R.J. (1996): Melt inclusion microthermometry: petrologic constraints from the H_2O-saturated haplogranite system. *Petrology* **4**, 291-306.

SUNAGAWA, I. (1992): In situ investigation of nucleation, growth, and dissolution of silicate crystals at high temperatures. *Annu. Rev. Earth Planet. Sci.* **20**, 113-142.

TAIT, S. (1992): Selective preservation of melt inclusions in igneous phenocrysts. *Am. Mineral.* **77**, 146-155.

THOMAS, R. & KLEMM, W. (1997): Microthermometric study of silicate melt inclusions in Variscan granites from SE Germany: volatile contents and entrapment conditions. *J. Petrol.* **38**, 1753-1765.

THOMAS, R., WEBSTER, J.D. & HEINRICH, W. (2000): Melt inclusions in pegmatite quartz: complete miscibility between silicate melts and hydrous fluids at low pressure. *Contrib. Mineral. Petrol.* **139**, 394-401.

THORNBER, C.R. (2001): Olivine-liquid relations of lava erupted by Kīlauea volcano from 1994 to 1998: implications for shallow magmatic processes associated with the ongoing East-Rift-Zone eruption. *Can. Mineral.* **39**, 239-266.

ZHAOLIN, L. (1994). The silicate melt inclusions in igneous rocks. *In* Fluid Inclusions in Minerals: Methods and Applications (B. De Vivo & M.L. Frezzotti, eds.). Virginia Polytechnic Institute and State University, Blacksburg, Virginia (73-94).

Received June 16, 2005, revised manuscript accepted May 21, 2006.